Anatomy of a flux transfer event seen by Cluster

B. U. Ö. Sonnerup
Dartmouth College, Hanover, New Hampshire, USA

H. Hasegawa
Dartmouth College, Hanover, New Hampshire, USA

G. Paschmann
Max-Planck-Institut für extraterrestrische Physik, Garching, Germany

Received 31 March 2004; revised 10 May 2004; accepted 12 May 2004; published 8 June 2004.

[1] Data from Cluster are used to study the structure of a flux transfer event (FTE), seen near the northern cusp. We employ Grad-Shafranov reconstruction, using measured fields from all four spacecraft to produce a map of the FTE cross section. The FTE consists of a flux rope of approximate size $1R_E$ and irregular shape, embedded in the magnetopause. Its axis $\hat{\mathbf{z}}$ is tangential to the magnetopause. Since no reconnection signatures are seen, the map provides a fossil record of the prior reconnection process that created the flux rope: the strong core field indicates that it was generated by component merging. An average reconnection electric field $\geq$0.18 mV/m must have occurred in the burst of reconnection that created the FTE. The total axial ($\hat{\mathbf{z}}$) current and magnetic flux in the FTE were -0.66 MAmp and +2.07 MWeber, respectively. *INDEX TERMS:* 2724 Magnetospheric Physics: Magnetopause, cusp, and boundary layers; 2784 Magnetospheric Physics: Solar wind/magnetosphere interactions; 7835 Space Plasma Physics: Magnetic reconnection. **Citation:** Sonnerup, B. U. Ö., H. Hasegawa, and G. Paschmann (2004), Anatomy of a flux transfer event seen by Cluster, *Geophys. Res. Lett.*, *31*, L11803, doi:10.1029/2004GL020134.

1. Introduction

[2] The fundamental signature of the passage of an FTE [*Russell and Elphic*, 1979], over an observing spacecraft, located near the magnetopause, is a bipolar pulse in the magnetic field normal to the unperturbed magnetopause surface. This signature is interpreted as the passage of a flux tube, embedded in the magnetopause and created by patchy and impulsive reconnection. Some events are remote encounters, sensed as a field deflection caused by field lines draping around the flux tube, and some are close encounters, caused by penetration of the observing spacecraft into the flux tube.

[3] We will apply Grad-Shafranov (GS) reconstruction for $2\frac{1}{2}$ dimensional magnetohydrostatic field/plasma structures to an FTE that has previously been studied by C. J. Owen (personal communication, 2003). The GS method yields a magnetic field map in the plane perpendicular to the axis of invariance of the structures and allows a complete description of them [*Hau and Sonnerup*, 1999; *Hu and Sonnerup*, 2000, 2003; *Hasegawa et al.*, 2004]. H. Hasegawa and B. U. Ö. Sonnerup (manuscript in preparation, 2004) have converted the method into a true multi-spacecraft technique in which data from all four Cluster spacecraft are ingested into the analysis, leading to the generation of a single optimal magnetic field map and invariant axis.

0094-8276/04/2004GL020134$05.00

2. Method

[4] The proper frame of the structure to be reconstructed is sliding along the magnetopause past the observing spacecraft. Additionally, it shares the inward/outward motion of the magnetopause. The speed of the structure relative to the spacecraft is determined as the deHoffmann-Teller (HT) frame velocity. In this frame, the plasma flow is as nearly field aligned as the velocities and magnetic fields, measured during the event, permit. The frame velocity, $\mathbf{V}_{HT}$, relative to the spacecraft, is obtained from a least squares procedure [e.g., *Khrabrov and Sonnerup*, 1998a].

[5] The reconstruction is based on the following three assumptions: (1) Inertia effects are negligible. This is the case if the plasma velocities in the HT frame are small compared with the Alfvén speed and the acoustic speed, but also for larger plasma speeds, when the field magnitude variations along field lines and the field-line curvature (and hence the streamline curvature) are small. The structure can then be considered magnetohydrostatic. (2) As seen in the HT frame, the structure is approximately time stationary. (3) The structure is elongated in some, initially unknown, direction, $\hat{\mathbf{z}}$, that we refer to as the invariant axis. The assumption $\partial/\partial z = 0$ is then adopted so that the structures we recover will be $2\frac{1}{2}$ dimensional. The magnetic field can now be expressed as $\mathbf{B} = (\partial A/\partial y, -\partial A/\partial x, B_z(x, y))$, where x and y are coordinates in the reconstruction plane, i.e., in the plane perpendicular to the invariant axis. Constant values of A describe field-line projections onto the $x-y$ plane and A is governed by the GS equation:

$$\partial^2 A/\partial x^2 + \partial^2 A/\partial y^2 = -\mu_0 dP_t/dA = -\mu_0 j_z \qquad (1)$$

[6] The quantity P_t is the transverse pressure, i.e., $P_t = (p + B_z^2/2\mu_0)$, and the plasma thermal pressure, p, as well as the axial field, B_z, are functions of A alone. It follows that P_t and the axial current density, j_z, are also functions of A alone. It is this property of the right-hand side of the GS equation that permits the reconstruction: If $P_t(A)$ and its derivative are known at one point along a field line having a particular value of A, then it is known at all points on that field line. But, as described below, $P_t(A)$ can be determined

from measured plasma pressures and fields at points along the projection of the spacecraft trajectory onto the $x-y$ plane; this projection is used as the x axis. Therefore the right hand side of the GS equation is known in all regions of the $x-y$ plane occupied by field lines that were encountered by the spacecraft, i.e., all field lines that crossed the x axis. In other parts of the $x-y$ plane, the field behavior must be recovered via suitable extrapolations of $P_t(A)$.

[7] The values of A along the projected spacecraft trajectory (the x axis) can be obtained from the measured field component, $B_y = -\partial A/\partial x$, by spatial integration,

$$A(x,0) = -\int B_y(x)dx, \tag{2}$$

which can be converted to time integration by the relation $dx = -V_{HTx}dt$. The outcome of this integration depends on the choice of the invariant axis, from which the x and y axes can then be obtained. In a single-spacecraft application, this choice is made by searching for an axis such that any field line, defined by a specific A value and encountered more than once along the spacecraft trajectory, leads to the same value of $P_t(A)$ at each intersection point [*Hau and Sonnerup*, 1999]. We shall determine the axis in a different manner, taking full advantage of multi-spacecraft information (H. Hasegawa and B. U. Ö. Sonnerup, manuscript in preparation, 2004).

[8] Once the function $P_t(A)$ has been found, the integration of the GS equation proceeds as follows: measured field components, B_x and B_y, at points along the trajectory are used as spatial initial values, allowing new values to be calculated by stepping away from the x axis in small steps, $\pm\Delta y$. For details about the integration procedure, about the suppression of numerical instabilities, and about validation against exact solutions of the GS equation, see the work by *Hau and Sonnerup* [1999] and *Hu and Sonnerup* [2003]. Validation by use of multi-spacecraft data has been performed by *Hu and Sonnerup* [2000] and by *Hasegawa et al.* [2004].

[9] H. Hasegawa and B. U. Ö. Sonnerup (manuscript in preparation, 2004) have developed a simple scheme for the construction of an optimal field map and axis orientation by ingestion of data from all four Cluster spacecraft. It contains the following elements: (1) A joint HT frame determination is made by merging data sets containing velocity measurements from the CIS/HIA instrument and magnetic field measurements from the FGM instrument onboard Cluster 1 (C1) and Cluster 3 (C3) (C2 and C4 lack CIS/HIA measurements). (2) Choice of a joint trial invariant axis is made, followed by determination of joint functions, $P_t(A)$ and $B_z(A)$. (3) Four magnetic field maps are produced, one from each spacecraft. In each map, the magnetic field from one spacecraft is used to initiate the GS integration. (4) In each map, the A value at each grid point is then weighted by a Gaussian function of y, centered at the spacecraft trajectory. The resulting four A values are then added at each point of a joint grid, the result being a combined map of A, i.e., of the magnetic field projected onto the $x-y$ plane. (5) The correlation coefficient between the field components this map predicts at points along each of the four spacecraft trajectories and the corresponding actually measured field components is calculated. It is then optimized by varying the choice of the invariant axis, the needed extrapolations of the functions $P_t(A)$ and $B_z(A)$, and the width of the Gaussian weight function. One arrives at the optimal map only after a large number of reconstructions have been performed. The optimal map no longer obeys the GS equation precisely. It accommodates deviations from the ideal model assumptions but preserves $\partial/\partial z = 0$. Once the optimum has been found, one can generate optimal functions $p(A)$, $N(A)$, $T(A)$, and $j_z(A) = dP_t(A)/dA$, needed for the generation of maps describing the plasma pressure, p, number density, N, temperature, T, and axial current density, j_z. Only the field and pressure maps will be presented here. The current density, $\mathbf{j}_t$, in the reconstruction plane is parallel to the magnetic field in that plane. It is given by $\mathbf{j}_t = (1/\mu_0)(dB_z/dA)\mathbf{B}_t$, where $\mathbf{B}_t = (B_x, B_y)$.

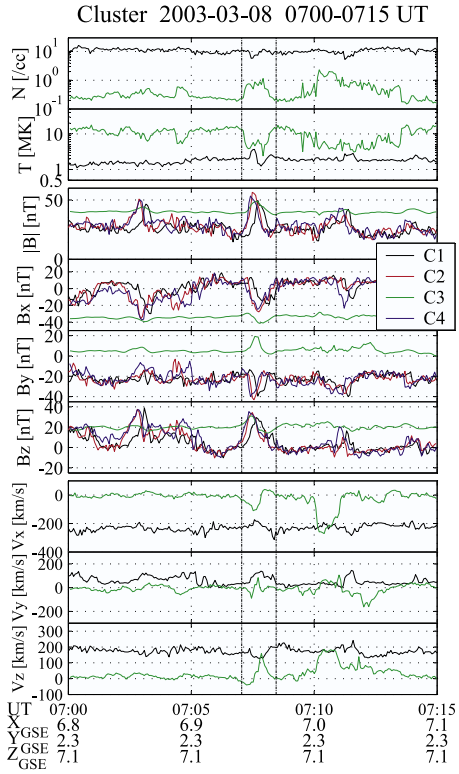

Figure 1. Cluster data on March 8, 2003, 0700–0715 UT. From top, the panels show: number density; temperature; field magnitude and GSE components; GSE velocity components. Time interval between the two vertical lines was used for the reconstruction.

3. FTE On March 8, 2003, 0708 UT

[10] The FTE to be reconstructed here was observed near the northern cusp: the GSE location was approximately (7.1, 2.5, 7.4) R_E and the spacecraft separations were about 5000 km. Figure 1 shows an overview of relevant data in a 15 min period surrounding the event. The interval between the two vertical lines was used in the reconstruction. Immediately before and after the event, C3 was located mainly in the magnetosphere whereas the other three spacecraft were measuring magnetosheath-like conditions. In the event itself, all spacecraft recorded a pronounced maximum in field magnitude. A peak in number density,

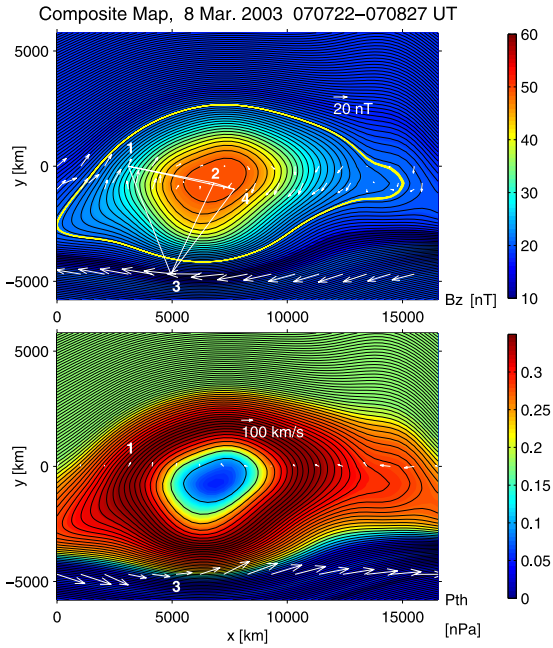

Figure 2. Reconstructed field lines projected onto the transverse plane, with axial magnetic field in color (top panel) or plasma pressure in color (bottom panel). In top panel, Cluster tetrahedron and measured transverse field, $\mathbf{B}_t = (B_x, B_y)$ are shown in white. In bottom panel, white arrows show measured transverse velocity in the HT frame. Equatorward edge of the map is to the right with magnetosphere on bottom. GSE coordinate axes of the map are x = (0.7338, −0.5896 −0.3375), y = (0.5940, 0.3158, 0.7399), z = (−0.3296, −0.7434, 0.5820).

accompanied by a minimum in temperature, was seen by C3, whereas C1 saw bipolar behavior at smaller amplitude. The HT frame velocity, obtained from the combined C1 and C3 data set, is (−234, 51, 166) km/s (GSE), i.e., the HT frame mainly moves anti-sunward and northward. The correlation coefficient between the GSE components of $\mathbf{V}_{HT} \times \mathbf{B}$ and the corresponding components of $\mathbf{v} \times \mathbf{B}$ is 0.938 ($\mathbf{v}$ denotes measured velocities). This relatively low value is a consequence of the fact that C1 and C3 separately gave somewhat different $\mathbf{V}_{HT}$ vectors. The slope of the regression line in the Walén plot (GSE velocity components, transformed to the HT frame, versus the corresponding components of the measured Alfvén velocities) was −0.16. This means that, relative to the Alfvén speed, there was only a small remnant, approximately field-aligned flow in the HT frame and no evidence of active reconnection. As discussed later on, the flow speed did exceed the sound speed at C3.

[11] The optimal field map is shown in the top panel of Figure 2, where field lines in the x–y plane are shown by black curves and the colors represent the axial (z) field component. White arrows with tails anchored at points along the four spacecraft trajectories, represent measured transverse fields. The low-latitude edge of the map is on the right and the magnetosphere is in the lower part. The yellow field-line loop contains a transverse magnetic flux per unit length along the z axis of 0.0549 Tm, an axial magnetic flux of $+2.07 \times 10^6$ Tm^2, and an axial current of $-0.66 \times 10^6 A$. This loop also shows that the FTE bulge is somewhat larger on the magnetosheath side than on the magnetosphere side.

[12] The lower panel in Figure 2 shows the same field lines but the colors now describe the thermal pressure and the white vectors represent transverse velocities, $\mathbf{v}'_t = (\mathbf{v} - \mathbf{V}_{HT})_t$, seen in the HT frame. These arrows are largest in the magnetosphere (C3), indicating that the HT frame is well anchored in the magnetosheath flow. The C3 velocity vectors are approximately aligned with the magnetic field, but not exactly so, as a consequence of the imperfect nature of the HT frame. The optimal invariant axis has GSE components $\hat{\mathbf{z}}$ = (−0.3296, −0.7434, +0.5820). This axis is very nearly perpendicular to a magnetopause normal, $\hat{\mathbf{n}}$ = (0.6444, 0.2446, 0.7245), derived from minimum variance analysis of the magnetic field during a magnetopause traversal by C1 around 0655 UT, the deviation being only 1.6°. In other words, the optimal axis is tangential to the magnetopause, as expected. It approximately bisects the angle of 117° between the fields on the two sides of the magnetopause. For distant encounters with an FTE, the invariant axis can also be obtained directly from the magnetic variance matrix [*Khrabrov and Sonnerup*, 1998b]. We have used this alternate method with the magnetic field data from C3 to obtain the axis (−0.3359, −0.6756, +0.6563) (GSE), which deviates from our optimal axis by only 5.8°.

[13] The correlation coefficient between the three GSE magnetic field components actually measured by each of the four spacecraft and the corresponding components predicted from the map was used in optimizing the map. As shown in Figure 3, the resulting correlation coefficient is high (cc = 0.990).

4. Discussion

[14] Several important items emerge from our study:

[15] 1. The high correlation coefficient for the reconstructed map indicates that many of its features are reliable. In particular, the orientation of the invariant axis has been accurately determined in the optimization process. It is then

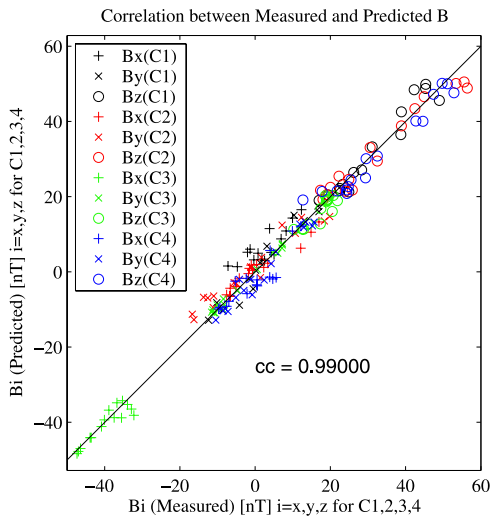

Figure 3. Field components along reconstruction coordinate axes (x, y, z), predicted by the map, versus those actually measured.

clear that this flux rope had a strong core field, which must have been created by a burst of component merging at some site equatorward of Cluster. Anti-parallel merging would not create any core field and therefore could not have been responsible for this FTE.

[16] 2. As shown in Figure 1, our FTE was preceded by another FTE some 5 minutes earlier. The amount of circumferential flux per unit axial length, 0.0549 Tm, contained within the yellow field-line loop in Figure 2, must have been reconnected during all, or a portion, of this 5-minute period, which implies an average reconnection electric field $-\langle E_z \rangle \geq 0.0549/300 = 0.183$ mV/m. In this calculation, we assume the creation and activation of a reconnection site (X line) equatorward of the observation point. The site then becomes inactive and is swept poleward, or perhaps starts moving first and then becomes inactive. About 5 minutes later the process is repeated.

[17] 3. The absence of reconnection signatures implies that, by the time the FTE reaches Cluster, it is nearly a fossil structure. It is in approximate force balance but is far from force free. Its rounded shape suggests that, during its travel to higher latitudes, it has deformed toward a minimum-energy configuration. The small, leftward velocities remaining in the HT frame, as seen by C1 toward the end of the event (in Figure 2 (bottom), on the right), indicates that the deformation process is not complete.

[18] 4. While the plasma flow speeds in the HT frame, seen by C1 as it traverses the FTE, are very small, this is not the case for C3 where the flow speeds are in fact supersonic. This means that important gas dynamic effects are present. In particular, the pressure, p, and the axial field, B_z, cannot be constant along a streamline (= field line), contrary to the situation described by the GS equation. Isentropic, field-aligned, supersonic but subalfvénic flow is such that the total and axial flow speed, Mach number, and axial field, $|B_z|$, all decrease, while the total field, pressure, density, and temperature increase, as the flow and field drape over the FTE bulge [*Sonnerup et al.*, 1992]. This behavior is seen in the data but, since C3 does not follow a flux tube, the variations could have been the result of penetration into the FTE. A portion of the density enhancement and temperature depression seen in the event was indeed caused by penetration into a boundary-layer region but the pressure peak and the B_z minimum both have considerably shorter duration than the density enhancement and occur at approximately constant entropy. Also, penetration into the FTE structure would cause $|B_z|$ to increase (see Figure 2), not decrease. Therefore, we believe the effects seen were in fact caused by supersonic field-aligned flow over a hump. Quantitative analysis of these effects will be presented elsewhere.

[19] 5. In Figure 1, the number density and temperature, seen by C1 as it traverses the FTE, do not deviate dramatically from their magnetosheath values. But their product, the plasma pressure, in fact exhibits interesting behavior, as seen in Figure 2 (bottom). The thermal pressure is enhanced in a ring-shaped region surrounding a central depression. This feature could result from expansion of the flux-rope cross section as the rope moves northward from the equatorial region into regions of lower external pressure. Or it could be a consequence of one end (or both ends) of the rope being magnetically connected to the inner magnetosphere and ionosphere. The ion distribution functions in the core show a cold population with $T_\perp > T_\parallel$, mixed with a hot, nearly isotropic, and more tenuous population. A useful diagnostic for connection to the ionosphere would be the simultaneous observation of PMAFs (poleward moving auroral forms).

[20] 6. Finally, we list a few questions about FTEs. Does component merging by necessity occur in a bursty fashion, leading to the generation of FTEs, or is the bursty behavior controlled by factors other than, or in addition to, the presence of a guide field? Does quasi-steady reconnection imply anti-parallel fields and/or vice versa? Are PMAFs a consequence of flux ropes (FTEs) with strong core fields, connected to the ionosphere? Antiparallel bursty reconnection would generate FTEs with little or no core field to connect to magnetospheric flux tubes with PMAFs at their ionospheric footpoints. PMAFs should therefore be absent when the IMF clock angle is near 180 degrees, as indeed they seem to be [*Sandholt et al.*, 2004].

[21] **Acknowledgments.** Discussions of PMAFs with N. Maynard, and assistance with plots of particle distributions from T.-D. Phan, are gratefully acknowledged. Research at Dartmouth College was supported by the National Aeronautics and Space Administration under Grant NAG5-12005.

References

Hasegawa, H., et al. (2004), Reconstruction of two-dimensional magnetopause structures from Cluster observations: Verification of method, *Ann. Geophys.*, *22*, 1251–1266.

Hau, L. N., and B. U. Ö. Sonnerup (1999), Two-dimensional coherent structures in the magnetopause: Recovery of static equilibria from single-spacecraft data, *J. Geophys. Res.*, *104*, 6899.

Hu, Q., and B. U. Ö. Sonnerup (2000), Magnetopause transects from two spacecraft: A comparison, *Geophys. Res. Lett.*, *7*, 1443.

Hu, Q., and B. U. Ö. Sonnerup (2003), Reconstruction of two-dimensional structures in the magnetopause: Method improvements, *J. Geophys. Res.*, *108*(A1), 1011, doi:10.1029/2002JA009323.

Khrabrov, A. V., and B. U. Ö. Sonnerup (1998a), DeHoffmann-Teller analysis, in *Analysis Methods for Multi-spacecraft Data*, *ISSI Sci. Rep. SR-001*, p. 221, Kluwer Acad., Norwell, Mass.

Khrabrov, A. V., and B. U. Ö. Sonnerup (1998b), Magnetic variance analysis for small amplitude waves and flux transfer events on a current sheet, *J. Geophys. Res.*, *103*, 11,907.

Russell, C. T., and R. C. Elphic (1979), ISEE observations of flux transfer events at the dayside magnetopause, *Geophys. Res. Lett.*, *6*, 33.

Sandholt, P. E., C. J. Farrugia, and W. F. Denig (2004), Dayside aurora and the role of IMF $|B_y|/|B_z|$: Detailed morphology and response to magnetopause reconnection, *Ann. Geophys.*, *22*, 613.

Sonnerup, B. U. Ö., L.-N. Hau, and D. W. Walthour (1992), On steady field-aligned double-adiabatic flow, *J. Geophys. Res.*, *97*, 12,015.

H. Hasegawa and B. U. Ö. Sonnerup, Thayer School of Engineering, Dartmouth College, 8000 Cummings Hall, Hanover, NH 03755, USA. (hasegawa@dartmouth.edu; sonnerup@dartmouth.edu)

G. Paschmann, Max-Planck-Institut für extraterrestrische Physik, Postfach 1312, D-85741 Garching, Germany. (goetz.paschmann@mpe.mpg.de)